bioRxiv preprint doi: https://doi.org/10.1101/2021.01.26.428356; this version posted January 27, 2021. The copyright holder for this preprint (which was not certified by peer review) is the author/funder, who has granted bioRxiv a license to display the preprint in perpetuity. It is made available under aCC-BY 4.0 International license.

1 # Sequence signatures of two IGHV3-53/3-66 public clonotypes to
2 # SARS-CoV-2 receptor binding domain

3

4 Timothy J.C. Tan[1,*], Meng Yuan[2,*], Kaylee Kuzelka[3], Gilberto C. Padron[3], Jacob R. Beal[3], Xin
5 Chen[1], Yiquan Wang[3], Joel Rivera-Cardona[4], Xueyong Zhu[2], Beth M. Stadtmueller[3],
6 Christopher B. Brooke[4,5], Ian A. Wilson[2,6,7,8,§], Nicholas C. Wu[1,3,5,§]

7

8 [1] Center for Biophysics and Quantitative Biology, University of Illinois at Urbana-Champaign,
9 Urbana, IL 61801, USA
10 [2] Department of Integrative Structural and Computational Biology, The Scripps Research
11 Institute, La Jolla, CA 92037, USA
12 [3] Department of Biochemistry, University of Illinois at Urbana-Champaign, Urbana, IL 61801,
13 USA
14 [4] Department of Microbiology, University of Illinois at Urbana-Champaign, Urbana, IL 61801,
15 USA
16 [5] Carl R. Woese Institute for Genomic Biology, University of Illinois at Urbana-Champaign,
17 Urbana, IL 61801, USA
18 [6] The Skaggs Institute for Chemical Biology, The Scripps Research Institute, La Jolla, CA
19 92037, USA
20 [7] IAVI Neutralizing Antibody Center, The Scripps Research Institute, La Jolla, CA 92037, USA
21 [8] Consortium for HIV/AIDS Vaccine Development (CHAVD), The Scripps Research Institute, La
22 Jolla, CA 92037, USA

23

24 * These authors contributed equally to this work.
25 [§]Correspondence: wilson@scripps.edu (I.A.W.) and nicwu@illinois.edu (N.C.W.)

bioRxiv preprint doi: https://doi.org/10.1101/2021.01.26.428356; this version posted January 27, 2021. The copyright holder for this preprint (which was not certified by peer review) is the author/funder, who has granted bioRxiv a license to display the preprint in perpetuity. It is made available under aCC-BY 4.0 International license.

26 **Abstract**

27 Since the COVID-19 pandemic onset, the antibody response to SARS-CoV-2 has been
28 extensively characterized. Antibodies to the receptor binding domain (RBD) on the spike protein
29 are frequently encoded by IGHV3-53/3-66 with a short CDR H3. Germline-encoded sequence
30 motifs in CDRs H1 and H2 play a major role, but whether any common motifs are present in CDR
31 H3, which is often critical for binding specificity, have not been elucidated. Here, we identify two
32 public clonotypes of IGHV3-53/3-66 RBD antibodies with a 9-residue CDR H3 that pair with
33 different light chains. Distinct sequence motifs on CDR H3 are present in the two public clonotypes
34 that appear to be related to differential light chain pairing. Additionally, we show that Y58F is a
35 common somatic hypermutation that results in increased binding affinity of IGHV3-53/3-66 RBD
36 antibodies with a short CDR H3. Overall, our results advance fundamental understanding of the
37 antibody response to SARS-CoV-2.

bioRxiv preprint doi: https://doi.org/10.1101/2021.01.26.428356; this version posted January 27, 2021. The copyright holder for this preprint (which was not certified by peer review) is the author/funder, who has granted bioRxiv a license to display the preprint in perpetuity. It is made available under aCC-BY 4.0 International license.

38 **Introduction**

39 Severe acute respiratory syndrome coronavirus-2 (SARS-CoV-2) is the etiological agent of
40 coronavirus disease 2019 (COVID-19)[1,2], which primarily results in respiratory distress, cardiac
41 failure, and renal injury in the most severe cases[3,4]. The virion is decorated with the spike (S)
42 glycoprotein, which contains a receptor-binding domain (RBD) that mediates virus entry by
43 binding to angiotensin-converting enzyme-2 (ACE-2) receptor on the surface of host cells[1,5-7]. To
44 mitigate the devastating social and economic consequences of the pandemic, vaccines and post-
45 exposure prophylaxes including antibody cocktails that exploit reactivity to the S protein are being
46 developed at an unprecedented rate. Several vaccines are currently in various stages of clinical
47 trials[8,9]. Most notable are the mRNA vaccines from Pfizer-BioNTech and Moderna, which have
48 been issued emergency use authorization by the Food and Drug Administration for distribution in
49 the United States[10-12] and the Oxford-AstraZeneca chimpanzee adenovirus vectored DNA vaccine
50 in the United Kingdom[13-15]. In humans, most neutralizing antibodies to SARS-CoV-2 target the
51 immunodominant RBD on the S protein[16,17], and can abrogate virus attachment and entry into
52 host cells[18,19]. In the past year, many RBD antibodies have been isolated and characterized from
53 convalescent SARS-CoV-2 patients [20-40].

54

55 Antibody diversity is generated through V(D)J recombination[41-43]. Three genes, one from each of
56 the variable (V), diversity (D) and joining (J) loci, are combined to form the coding region for the
57 heavy chain. In humans, genes encoding for the V, D and J regions are denoted as IGHV, IGHD
58 and IGHJ, respectively. Two complementarity-determining regions on the heavy chain (CDRs H1
59 and H2) are encoded by the V gene while the third (CDR H3) is encoded by the V(D)J junction. A
60 similar process occurs in assembly of the coding region for the light chain except that the D gene
61 is absent. The light chain genes also encode kappa and lambda chains that are denoted as IGKV
62 and IGKJ, as well as IGLV and IGLJ, respectively. To further improve affinity of antibodies to an
63 antigen, affinity maturation occurs via somatic hypermutation (SHM)[44,45]. V(D)J recombination and

bioRxiv preprint doi: https://doi.org/10.1101/2021.01.26.428356; this version posted January 27, 2021. The copyright holder for this preprint (which was not certified by peer review) is the author/funder, who has granted bioRxiv a license to display the preprint in perpetuity. It is made available under aCC-BY 4.0 International license.

64 SHM therefore ensure a diverse repertoire of antibodies is available for an immune response to
65 the enormous number and variety of potential antigens.
66
67 Notwithstanding this antibody diversity, some RBD antibodies with strikingly similar sequences
68 have been found in multiple convalescent SARS-CoV-2 patients[32,46,47]. These antibodies can be
69 classified as public clonotypes if they share the same IGHV gene with similar CDR H3
70 sequences[48-52]. Over the past decade, public clonotypes to human immunodeficiency virus[48],
71 malaria[52], influenza[49], and dengue virus[53] have been discovered. Antibodies to SARS-CoV-2 RBD
72 frequently use IGHV3-53 and IGHV3-66[23,31,47,54], which only differ by one amino acid (i.e. I12 in
73 IGHV3-53 and V12 in IGHV3-66). IGHV3-53/3-66 antibodies carry germline-encoded features
74 that are critical for RBD binding – an NY motif in CDR H1 and an SGGS motif in CDR H2[31,47,54].
75 Nevertheless, IGHV3-53/3-66 RBD antibodies have varying lengths of CDR H3 with diverse
76 sequences, which seem to deviate from the canonical definition of a public clonotype.
77
78 By categorizing IGHV3-53/3-66 RBD antibodies based on CDR H3 length and light chain usage,
79 we now report on two public clonotypes of IGHV3-53/3-66 RBD antibodies, both of which have a
80 CDR H3 length of 9 amino acids but with distinct sequence motifs. Our structural and biochemical
81 analyses reveal that these sequence motifs on CDR H3 are associated with light chain pairing
82 preference. We also identify Y58F as a signature SHM among IGHV3-53/3-66 RBD antibodies
83 that have a CDR H3 length of less than 15 amino acids (Kabat numbering). As the COVID-19
84 pandemic continues, knowledge of public antibodies against SARS-CoV-2 can inform on
85 therapeutic development as well as vaccine assessment.
86
87 **Results**
88 **Two public clonotypes of IGHV3-53/3-66 RBD antibodies**

bioRxiv preprint doi: https://doi.org/10.1101/2021.01.26.428356; this version posted January 27, 2021. The copyright holder for this preprint (which was not certified by peer review) is the author/funder, who has granted bioRxiv a license to display the preprint in perpetuity. It is made available under aCC-BY 4.0 International license.

89 In this study, we define clonotypic IGHV3-53/3-66 RBD antibodies as antibodies that share the
90 same IGL(K)V genes and with identical CDR H3 length. Literature mining of 214 published
91 IGHV3-53/3-66 RBD antibodies obtained from convalescent patients (Supplementary Table 1)
92 revealed that the two most common clonotypes have a CDR H3 length of 9 amino acids and are
93 paired with light chains IGKV1-9 (clonotype 1) and IGKV3-20 (clonotype 2), respectively (Figure
94 1a). Antibodies from clonotype 1 have been observed across 10 studies[22-24,32-36,40], whereas
95 antibodies from clonotype 2 are found across seven studies[22,24,32-34,37,40]. Interestingly, sequence
96 logos revealed distinct sequence features of CDR H3 between clonotype 1 and clonotype 2
97 antibodies (Figure 1b).
98
99 We further determined IGHJ gene usage in the two major clonotypes of IGHV3-53/3-66 RBD
100 antibodies. Among the IGHV3-53/3-66 RBD antibodies with a CDR H3 length of 9 amino acids,
101 we observed a statistically significant bias in IGHJ gene usage (p-value = 2e-6, Fisher's exact
102 test), where clonotypes 1 and 2 preferentially pair with IGHJ6 and IGHJ4, respectively (Figure
103 1c). In fact, IGHJ6 encodes the last four amino acids (GMDV) in CDR H3 that are highly conserved
104 in clonotype 1 (Figure 1d, Supplementary Figure 1a). Similarly, IGHJ4 encodes the last four amino
105 acids (YFDY) in CDR H3 that are highly conserved in clonotype 2 (Figure 1d, Supplementary
106 Figure 1b). Taken together, we demonstrate that IGHV3-53/3-66 RBD antibodies can be
107 categorized into at least two public clonotypes.
108

109 **Structural analysis of signature motifs on CDR H3**

110 We further investigated sequence signatures of CDR H3s in clonotypes 1 and 2 (Figure 1b). In
111 particular, we focused on amino acid residues 96, 98 and 100 in CDR H3 since these residues
112 show clear patterns of differential amino-acid preference between clonotype 1 and clonotype 2
113 antibodies. Subsequently, analysis was performed on structures of BD-604 (PDB 7CH4) and

bioRxiv preprint doi: https://doi.org/10.1101/2021.01.26.428356; this version posted January 27, 2021. The copyright holder for this preprint (which was not certified by peer review) is the author/funder, who has granted bioRxiv a license to display the preprint in perpetuity. It is made available under aCC-BY 4.0 International license.

114 CC12.1 (PDB 6XC2), which are two clonotype 1 antibodies, as well as BD-629 (PDB 7CH5) and
115 CC12.3 (PDB 6XC4), which are two clonotype 2 antibodies.
116
117 Residue 96 is usually Leu in clonotype 1 antibodies, while an aromatic residue, usually Tyr,
118 occupies residue 96 in clonotype 2 antibodies. While V_H L96 interacts with Y489 of the RBD in
119 clonotype 1 antibodies via van der Waals interactions, V_H F/Y96 is located at the center of a π–π
120 stacking network that involves F456, Y489 and V_H Y100 (Figure 2a, 2b, Supplementary Figure
121 2a, 2b; left panels). Substituting V_H L96 in clonotype 1 with Y96 would result in a clash with RBD
122 Y489, whereas substituting V_H F/Y96 in clonotype 2 with L96 would abolish the π–π stacking
123 network but still maintain a hydrophobic core.
124
125 Residue 98 in CDR H3 of clonotype 1 antibodies does not show a strong amino-acid preference,
126 since it is located in a relatively open space (Figure 1b, 2a, Supplementary Figure 2a; middle
127 panels). On the other hand, a highly conserved acidic residue at position 98 in the CDR H3 loop
128 of clonotype 2 antibodies contributes to formation of hydrogen bond interactions with V_H Y52 as
129 well as electrostatic interactions with RBD K417 and V_L R96 (Figure 2b, Supplementary Figure
130 2b; middle panels). Consistently, V_L R96 is highly conserved in clonotype 2 antibodies, but not in
131 other IGHV3-53/3-66 RBD antibodies (Supplementary Figure 3). Thus, the electrostatic
132 interactions between V_H D/E98 and V_L R98 are highly conserved in clonotype 2 antibodies and
133 can likely help stabilize the CDR H3 loop conformation to minimize entropic cost upon binding to
134 SARS-CoV-2 RBD.
135
136 Residue 100 is usually Gly in CDR H3 of clonotype 1 antibodies (Figure 1b). Structural analysis
137 shows that small, non-polar amino acids are favored at position 100 due to the limited space
138 around that residue (Figure 2a, Supplementary Figure 2a; right panels). Moreover, G100 in

bioRxiv preprint doi: https://doi.org/10.1101/2021.01.26.428356; this version posted January 27, 2021. The copyright holder for this preprint (which was not certified by peer review) is the author/funder, who has granted bioRxiv a license to display the preprint in perpetuity. It is made available under aCC-BY 4.0 International license.

139 clonotype 1 has a positive Φ angle, which is typically less favorable for non-Gly amino acids. In
140 contrast, residue 100 is a highly conserved Tyr in CDR H3 of clonotype 2 antibodies (Figure 1b).
141 Structural analysis shows that V_H Y100 contributes to the $\pi-\pi$ stacking network that is formed via
142 the aromatic ring at V_H residue 96 (see above) and an aromatic residue at V_L residue 49 (Figure
143 2b, Supplementary Figure 2b; right panels).
144
145 Additionally, we investigated the structural basis of the conservation of V_H Y102 among clonotype
146 2 antibodies. Structural analysis reveals that V_H Y102 interacts with RBD Y486 via $\pi-\pi$
147 interactions (Supplementary Figure 4). Only IGHJ4 offers a bulky aromatic side chain at residue
148 102 (Figure 1d), which explains the common usage of IGHJ4 in clonotype 2 antibodies. In
149 contrast, clonotype 1 antibodies frequently use IGHJ6 (Figure 1d), which has a much shorter Val
150 at residue 102, most likely because IGHJ6 encodes a Gly at residue 100 that can avoid steric
151 clashes with the light chain (see above, Figure 2a, Supplementary Figure 2a; right panels). Of
152 note, the only other IGHJ gene that encodes a non-bulky amino acid at residue 100 is IGHJ3
153 (Ala). IGHJ1, IGHJ2, IGHJ4, and IGHJ5 all encode a bulky residue at residue 100 (Figure 1d),
154 which may be disfavored in clonotype 1 antibodies due to the limited space where V_H residue 100
155 is located (Supplementary Figure 5). Overall, our structural analyses provide a structural basis for
156 the differential signature sequence motifs in CDR H3 between clonotype 1 and clonotype 2
157 antibodies.
158
159 **Incompatibility of CDR H3 between clonotype 1 and clonotype 2 antibodies**
160 To understand the influence of light-chain usage in CDR H3 sequences, we performed a structural
161 alignment of RBD-bound CDR H3 from two clonotype 1 antibodies, namely BD-604 and CC12.1,
162 and two clonotype 2 antibodies, namely BD-629 and CC12.3 (Supplementary Figures 2c-2f).
163 While the CDR H3 conformations are similar within each clonotype (RMSD ranges from 0.27 to

bioRxiv preprint doi: https://doi.org/10.1101/2021.01.26.428356; this version posted January 27, 2021. The copyright holder for this preprint (which was not certified by peer review) is the author/funder, who has granted bioRxiv a license to display the preprint in perpetuity. It is made available under aCC-BY 4.0 International license.

164 0.41 Å), they are quite different between clonotypes (RMSD ranges from 0.77 Å to 1.5 Å).
165 Although our sample size is small, this analysis suggests that antibodies from clonotypes 1 and
166 2 have different preferences for their CDR H3 conformations. Such differential preference of CDR
167 H3 conformations may be partly influenced by light-chain usage, as indicated by the structural
168 analyses above on V_H residues 96, 98, and 100 (Figure 2, Supplementary Figures 2 and 5).
169

170 To experimentally examine the compatibility between CDR H3 and the light chains from clonotype
171 1 and clonotype 2 antibodies, we focused on antibodies COV107-23 (clonotype 1) and COVD21-
172 C8 (clonotype 2). The heavy-chain sequences of these two antibodies only differ by four amino
173 acids in CDR H3, namely V_H residues 96, 98, 99, and 100 (Supplementary Figure 6a). Of note,
174 COV107-23 uses IGHJ4, which is seldom observed among clonotype 1 antibodies but highly
175 preferred in clonotype 2 antibodies (Figure 1c), to encode the two amino acids at the C-terminus
176 of its CDR H3 (Supplementary Figure 6b). Both COV107-23 and COVD21-C8 bind strongly to the
177 SARS-CoV-2 RBD, with dissociation constants (K_D) of 1 nM and 4 nM, respectively (Figure 3a).
178 However, when their light chains are swapped, their binding affinity to the RBD is weakened
179 substantially to K_D > 1 μM. We further determined apo crystal structures of COV107-23 paired
180 with its native light chain and with the light chain from COVD21-C8 to 2.0 Å and 3.3 Å, respectively
181 (Supplementary Table 2). The conformations of CDR H3 indeed differ when paired with different
182 light chains, as exemplified by the 3.3 Å displacement of V_H G97 near the tip of CDR H3 and
183 different side-chain orientations of V_H T98 (Figure 3b). In addition, a type I' β-turn is observed at
184 the tip of CDR H3 in COV107-23 when paired with its native light chain but not with the light chain
185 from COVD21-C8 (Figure 3c). These observations demonstrate that the conformation of CDR H3
186 changes substantially when IGKV1-9 in COV10-23 is swapped to IGKV3-20, which abolishes the
187 binding to RBD (Figure 3a). The CDR H3 conformation is therefore a determinant for compatibility
188 between the CDR H3 sequence and the light chain in IGHV3-53/3-66 RBD antibodies.
189

bioRxiv preprint doi: https://doi.org/10.1101/2021.01.26.428356; this version posted January 27, 2021. The copyright holder for this preprint (which was not certified by peer review) is the author/funder, who has granted bioRxiv a license to display the preprint in perpetuity. It is made available under aCC-BY 4.0 International license.

190 **Compatibility of different CDR H3 variants with IGHV1-9 for binding to RBD**

191 Besides antibodies from clonotypes 1 and 2, other IGHV3-53/3-66 RBD antibodies with a range
192 of CDR H3 lengths pair with different light chains (Figure 1a). We further aimed to expand our
193 analysis on CDR H3 compatibility to include CDR H3 from IGHV3-53/3-66 RBD antibodies other
194 than clonotypes 1 and 2. In particular, we focused on identifying CDR H3 sequences that are
195 compatible with IGKV1-9, which is used by clonotype 1 antibodies for binding to RBD. We first
196 compiled a list of 143 CDR H3 variants that were observed in IGHV3-53/3-66 RBD antibodies
197 (Supplementary Table 3). A yeast display library was then constructed with these 143 CDR H3
198 variants in the B38 antibody, which is a IGHV3-53/IGKV1-9 RBD antibody[26]. Subsequently,
199 fluorescence-activated cell sorting (FACS) was performed on the yeast display library based on
200 antibody expression level and binding to SARS-CoV-2 RBD (Supplementary Figures 7 and 8).
201 The enrichment level of each CDR H3 variant in the sorted library was quantified by next-
202 generation sequencing (see Methods, Supplementary Table 4). CDR H3 variants that were
203 positively enriched in binding ($\log_{10}$ enrichment > 0) are derived from both IGKV1-9 and non-
204 IGKV1-9 antibodies (Figure 4a). The native CDR H3 for B38 has a $\log_{10}$ enrichment level of -
205 0.002. As a result, positively enriched CDR H3 variants should have a higher affinity than wild-
206 type B38. A total of 68% (17 out of 25) binding-enriched CDR H3 variants have a length of 9
207 amino acids, whereas only 31% (37 out of 118) have a length of 9 amino acids in the non-enriched
208 group (Figure 4b). Interestingly, binding-enriched CDR H3 variants with a length of 9 amino acids
209 displayed very similar sequence features as that of clonotype 1 antibodies obtained from literature
210 mining (Figure 1b and 4c). Of note, 41% (7 out of 17) binding-enriched CDR H3 variants with a
211 length of 9 amino acids come from non-IGKV1-9 antibodies. Overall, our yeast display screen
212 indicates that certain CDR H3s from non-IGKV1-9 RBD antibodies are compatible with IGKV1-9
213 for RBD binding and have similar sequence features as those CDR H3s from clonotype 1
214 antibodies.

215

bioRxiv preprint doi: https://doi.org/10.1101/2021.01.26.428356; this version posted January 27, 2021. The copyright holder for this preprint (which was not certified by peer review) is the author/funder, who has granted bioRxiv a license to display the preprint in perpetuity. It is made available under aCC-BY 4.0 International license.

216 We noticed that some CDR H3 sequences that come from IGKV1-9 RBD antibodies do not enrich
217 in binding. One possibility is that they are still able to bind to RBD, but with a lower affinity than
218 B38, which has a K_D of 70 nM to the RBD[26]. However, as shown by our yeast display screen,
219 CDR H3 sequences from IGKV1-9 antibodies in general have a significantly stronger binding to
220 RBD than those from non-IGKV1-9 antibodies (p-value = 0.002, Figure 4d), whereas their
221 expression level is only marginally higher than that from non-IGKV1-9 antibodies (p-value = 0.06,
222 Figure 4d).
223

224 **Y58F is a signature SHM in IGHV3-53/3-66 RBD antibodies**

225 We further aimed to understand if there are common SHMs among IGHV3-53/3-66 RBD
226 antibodies. We first categorized IGHV3-53/3-66 RBD antibodies from convalescent SARS-CoV-
227 2 patients by CDR H3 length. The occurrence frequencies of individual SHMs in each category
228 were then analyzed (Figure 5a). This analysis included 214 IGHV3-53/3-66 RBD antibodies that
229 have sequence information available. One clear observation is that Y58F is highly common
230 among IGHV3-53/3-66 RBD antibodies with a CDR H3 length of less than 15 amino acids, but
231 completely absent when the CDR H3 length is 15 amino acids or above, suggesting that Y58F
232 improves the binding of affinity IGHV3-53/3-66 antibodies to RBD only when they have a short
233 CDR H3 loop (CDR H3 < 15 amino acids). To understand the effect of Y58F on the binding affinity
234 of IGHV3-53/3-66 antibodies to the RBD, we compared the binding affinity of the same antibodies
235 that carry either Y58 or F58 to the RBD. In particular, we focused on three IGHV3-53/3-66 RBD
236 antibodies that have a CDR H3 length of 9 amino acids – one in clonotype 1 (COV107-23), and
237 two in clonotype 2 (COVD21-C8 and CC12.3). Our BLI experiments showed that the Y58F
238 mutation dramatically improved the affinity of the three antibodies (COV107-23, COVD21-C8 and
239 CC12.3) by ~10-fold to ~1000-fold (Figure 5b, Supplementary Figure 9). As a control, we also
240 performed the same experiment on an IGHV3-53/3-66 antibody with a CDR H3 length of 15 amino
241 acids, namely COVA2-20. In contrast to those three IGHV3-53/3-66 RBD antibodies with a short

bioRxiv preprint doi: https://doi.org/10.1101/2021.01.26.428356; this version posted January 27, 2021. The copyright holder for this preprint (which was not certified by peer review) is the author/funder, who has granted bioRxiv a license to display the preprint in perpetuity. It is made available under aCC-BY 4.0 International license.

242 CDR H3, COVA2-20 shows similar binding affinity to RBD between Y58 and F58 variants (Figure
243 5b, Supplementary Figure 5). Taken together, our results show that Y58F appears to be a
244 signature SHM in IGHV3-53/3-66 RBD antibodies with CDR H3 length of < 15 amino acids. In
245 fact, the results here are consistent with our previous finding that IGHV3-53/3-66 RBD antibodies
246 with CDR H3 length of 15 amino acids or longer adopt a different binding mode as compared to
247 those with a shorter CDR H3[54].
248
249 Interestingly, a Y58F mutation results in a loss of hydrogen bonding interactions between residue
250 58 of the heavy chain and T415 of the RBD (Supplementary Figure 10), yet the mutation
251 significantly increases the binding affinity of the antibody to the RBD. We then performed a
252 structural analysis on seven IGHV3-53/66 RBD antibodies with Y58F mutation and nine
253 without[26,29,38,40,47,54-57]. Our results indicate that, by removal of the hydroxyl group, the side chain
254 of Y58F moves closer to the backbone carbon of RBD T415 (Supplementary Figure 10). The
255 average distance between the centroid of the side-chain aromatic ring at V_H residue 58 and the
256 backbone carbon of RBD T415 are 5.3 Å and 5.9 Å for antibodies that carry F58 and Y58,
257 respectively. Since T-shaped π-π stacking is optimal at around 5.0 to 5.2 Å[58,59], F58 but not Y58
258 can form strong T-shaped π-π stacking interactions with the amide backbone of RBD T415. This
259 observation can at least partly explain why Y58F improves affinity despite the loss of a hydrogen
260 bond with the RBD.
261

262 **Discussion**

263 While several studies to date have described IGHV3-53/3-66 as a commonly used germline for
264 SARS-CoV-2 RBD antibodies[23,31,47,54], the exact sequence requirements for generating an
265 IGHV3-53/3-66 antibody to SARS-CoV-2 RBD has remained largely elusive. As a result of
266 numerous efforts from multiple groups in isolating RBD antibodies and reporting their

bioRxiv preprint doi: https://doi.org/10.1101/2021.01.26.428356; this version posted January 27, 2021. The copyright holder for this preprint (which was not certified by peer review) is the author/funder, who has granted bioRxiv a license to display the preprint in perpetuity. It is made available under aCC-BY 4.0 International license.

267 sequences[20-40], detailed characterization of RBD antibody sequence features has become
268 possible. Through sequence analysis, biophysical experiments, and high-throughput screening,
269 we identified distinct sequence requirements for two public clonotypes (clonotypes 1 and 2) of
270 IGHV3-53/3-66 RBD antibodies. In fact, the frequent occurrence of IGHV3-53/3-66 RBD
271 antibodies with IGHJ6 and a CDR H3 length of 9 amino acids, which are germline features of
272 clonotype 1 antibodies, have also been reported in previous publications[23,60].
273
274 One important finding in this study is that the CDR H3 sequence that supports IGHV3-53/3-66
275 antibodies binding to RBD is light chain-dependent. This finding is consistent with our previous
276 observation that there is a large diversity of CDR H3 sequences in IGHV3-53/3-66 RBD
277 antibodies[54]. In addition, our findings explain a recent observation by Banach and colleagues[61]
278 who showed that swapping the heavy and light chains of different IGHV3-53/3-66 RBD antibodies
279 often substantially reduced their neutralization potency. Therefore, IGHV3-53/3-66 provides a
280 robust framework to generate different public clonotypes that have distinct CDR H3 and light chain
281 sequence signatures. While only two major clonotypes of IGHV3-53/3-66 RBD antibodies are
282 examined in this study, it will be worth characterizing other minor clonotypes to obtain a more
283 complete understanding of the compatibility between CDR H3 sequence and light-chain identity
284 among IGHV3-53/3-66 RBD antibodies.
285
286 Although this study revealed that Y58F is a common SHM that improves the affinity of IGHV3-
287 53/3-66 antibodies with a short CDR H3 to RBD, other common SHMs have also shown up in our
288 sequence analysis (Figure 5a), albeit with a lower frequency. Most noticeably, a cluster of
289 common SHMs is found in V_H framework region 1 from residues 26 to 28. This cluster of SHMs
290 is also likely to be important for affinity maturation to RBD. A recent study has indeed shown that
291 SHMs V_H F27V and T28I together increase affinity by 100-fold of an IGHV3-53/3-66 antibody to
292 the SARS-CoV-2 RBD[38]. Additional common SHMs among IGHV3-53/3-66 RBD antibodies with

bioRxiv preprint doi: https://doi.org/10.1101/2021.01.26.428356; this version posted January 27, 2021. The copyright holder for this preprint (which was not certified by peer review) is the author/funder, who has granted bioRxiv a license to display the preprint in perpetuity. It is made available under aCC-BY 4.0 International license.

293 a short CDR H3 include S31R in CDR H1 and V50L in CDR H2 (Figure 5a). As a result, while
294 IGHV3-53/3-66 RBD antibodies do not require any SHM to neutralize SARS-CoV-2[57], this study
295 along with others have shown that SHM can substantially improve the binding affinity of IGHV3-
296 53/3-66 antibodies to RBD[38,57]. Consistently, RBD antibodies from convalescent SARS-CoV-2
297 patients have significantly more SHMs and higher neutralization potency at 6 months post-
298 infection than at 1-month post-infection[62].
299
300 Circulating SARS-CoV-2 mutant variants represent a major ongoing challenge to natural immunity
301 and vaccination. In particular, a lot of attention has been focused on RBD mutation E484K, which
302 has emerged in multiple independently SARS-CoV-2 lineages[63,64] and can alter the antigenicity
303 of the spike protein[65-67]. Another naturally occurring RBD mutation, K417N, which has emerged
304 in South Africa and Brazil (B.1.351 lineage and B.1.1.28, respectively)[63,64,68], has recently been
305 shown to also alter antigenicity of the spike protein[66,69-71]. Consistently, we found that K417N
306 dramatically decreased the binding of COV107-23 (clonotype 1) and COVD21-C8 (clonotype 2)
307 to RBD (Supplementary Figures 11a-11b). In fact, K417 forms an electrostatic interaction with the
308 signature residue V_H D/E98 of CDR H3 in clonotype 2 antibodies (Figure 2b) and can also interact
309 with CDR H3 of clonotype 1 antibodies (Supplementary Figure 11c), providing a structural
310 explanation for its change in antigenicity. Constant antigenic drift of SARS-CoV-2 is unavoidable
311 if it keeps circulating among humans. Thus, sustained efforts in characterizing the antibody
312 response to SARS-CoV-2 as it evolves will not only benefit vaccine development and assessment,
313 but also improve our fundamental understanding of the ability of the antibody repertoire to rapidly
314 respond to viral infections.

bioRxiv preprint doi: https://doi.org/10.1101/2021.01.26.428356; this version posted January 27, 2021. The copyright holder for this preprint (which was not certified by peer review) is the author/funder, who has granted bioRxiv a license to display the preprint in perpetuity. It is made available under aCC-BY 4.0 International license.

315 **Methods**

316 **Literature mining for antibodies to SARS-CoV-2 RBD**

317 Sequences of anti-SARS-CoV-2 RBD from convalescent patients infected with SARS-CoV-2
318 were obtained from published articles[20-40] (Supplementary Table 1). IgBlast was used to identify
319 somatic hypermutations and analyze IGHJ gene usage[72]. Of note, IgBlast can only identify IGHJ
320 gene usage for antibodies with available nucleotide sequences. Sequence logos were generated
321 by WebLogo[73].

322

323 **Expression and purification of Fc-tagged RBD**

324 The receptor-binding domain (RBD) (residues 319-541) of the SARS-CoV-2 spike (S) protein
325 (GenBank: QHD43416.1) was fused with an N-terminal Igk secretion signal and a C-terminal
326 SSSSG linker followed by an Fc tag and cloned into a phCMV3 vector. The plasmid was
327 transiently transfected into Expi293F cells using ExpiFectamine™ 293 Reagent (Thermo Fisher
328 Scientific) according to the manufacturer's instructions. The supernatant was collected at 7 days
329 post-transfection. The Fc-tagged RBD was purified with by KanCapA protein A affinity resin
330 (Kaneka).

331

332 **Expression and purification of Fabs**

333 Fab heavy and light chains were cloned into phCMV3. Heavy chain Y58F or F58Y mutants were
334 constructed using the QuikChange XL Mutagenesis kit (Stratagene) according to the
335 manufacturer's instructions. The plasmids were transiently co-transfected into Expi293F cells at
336 a ratio of 2:1 (HC:LC) using ExpiFectamine™ 293 Reagent (Thermo Fisher Scientific) according
337 to the manufacturer's instructions. The supernatant was collected at 7 days post-transfection. The
338 Fab was purified with a CaptureSelect™ CH1-XL Pre-packed Column (Thermo Fisher Scientific).

339

340 **Biolayer interferometry binding assay**

bioRxiv preprint doi: https://doi.org/10.1101/2021.01.26.428356; this version posted January 27, 2021. The copyright holder for this preprint (which was not certified by peer review) is the author/funder, who has granted bioRxiv a license to display the preprint in perpetuity. It is made available under aCC-BY 4.0 International license.

341 Binding assays were performed by biolayer interferometry (BLI) using an Octet Red96e
342 instrument (FortéBio) as described previously[74]. Briefly, Fc-tagged SARS-CoV-2 RBD proteins at
343 20 to 100 μg/ml in 1x kinetics buffer (1x PBS, pH 7.4, 0.01% w/v BSA and 0.002% v/v Tween 20)
344 were loaded onto streptavidin (SA) biosensors and incubated with the indicated concentrations of
345 Fabs. The assay consisted of five steps: 1) baseline: 60 s with 1x kinetics buffer; 2) loading: 300 s
346 with His_6-tagged S or RBD proteins; 3) baseline: 60 s with 1x kinetics buffer; 4) association: 60 s
347 with samples (Fab or IgG); and 5) dissociation: 60 s with 1x kinetics buffer. For estimating the
348 exact K_D, a 1:1 binding model was used.
349

350 **X-ray crystallography**

351 Fabs COV107-23 (15 mg/ml) and COV107-23 paired with the light chain of COVD21-C8
352 (COV107-23-swap, 14 mg/ml) were screened for crystallization using the 384 conditions of the
353 JCSG Core Suite (Qiagen) on our custom-designed robotic CrystalMation system (Rigaku) at
354 Scripps Research by the vapor diffusion method in sitting drops containing 0.1 μl of protein and
355 0.1 μl of reservoir solution. For COV107-23, optimized crystals were grown in 0.085 M of sodium
356 citrate - citric acid pH 5.6, 0.17 M ammonium acetate, 15% (v/v) glycerol, and 25.5% (w/v)
357 polyethylene glycol 4000 at 20°C. For COV107-23-swap, optimized crystals were grown in 0.1 M
358 of sodium citrate pH 4, 1 M lithium chloride, and 20% (w/v) polyethylene glycol 6000 at 20°C.
359 Crystals were grown for 7 days and then harvested and flash cooled in liquid nitrogen. Diffraction
360 data were collected at cryogenic temperature (100 K) at Stanford Synchrotron Radiation
361 Lightsource (SSRL) on the Scripps/Stanford beamline 12-1 with a beam wavelength of 0.97946
362 Å, and processed with HKL2000[75]. Structures were solved by molecular replacement using
363 PHASER[76], where the models were generated by Repertoire Builder
364 (https://sysimm.org/rep_builder/)[77]. Iterative model building and refinement were carried out in
365 COOT[78] and PHENIX[79], respectively.
366

bioRxiv preprint doi: https://doi.org/10.1101/2021.01.26.428356; this version posted January 27, 2021. The copyright holder for this preprint (which was not certified by peer review) is the author/funder, who has granted bioRxiv a license to display the preprint in perpetuity. It is made available under aCC-BY 4.0 International license.

367 **Construction of plasmids and CDR H3 library**

368 143 oligonucleotides (Supplementary Table 3) encoding CDR H3 were obtained from Integrated
369 DNA Technologies (IDT) and PCR-amplified using 5´-ACC TAC AGA TGA ATT CTC TTA GGG
370 CAG AAG ATA CCG CCG TCT ACT ACT GC-3´ as forward primer and 5´-GGG CCT TTT GTA
371 GAA GCT GAA CTC ACA GTG ACG GTA GTC CCT TGT CCC CA-3´ as reverse primer. Then,
372 the amplified oligonucleotide pool was gel-purified using a GeneJET Gel Extraction Kit (Thermo
373 Scientific).

374

375 Wild-type (WT) B38 yeast display plasmid, pCTcon2_B38, was generated by cloning the coding
376 sequence of (from N-terminal to C-terminal, all in-frame) Aga2 secretion signal, B38 Fab light
377 chain, V5 tag, ERBV-1 2A self-cleaving peptide, Aga2 secretion signal, B38 Fab heavy chain, HA
378 tag, and Aga2p, into the pCTcon2 vector[80]. pCTcon2_B38 was PCR-amplified using 5´-TGG GGA
379 CAA GGG ACT ACC GTC ACT GTG-3´ as forward primer and 5´-GCA GTA GTA GAC GGC
380 GGT ATC TTC TGC-3´ as reverse primer to generate the linearized vector. The PCR product was
381 then gel-purified.

382

383 **Yeast antibody display library generation**

384 5 μg of the amplified oligonucleotide pool and 4 μg of purified linearized vector were transformed
385 into *Saccharomyces cerevisiae* EBY100 via electroporation following previously published
386 protocol[81] to generate a B38 yeast display library with different CDR H3 variants.

387

388 **Fluorescence-activated cell sorting of yeast antibody display library**

389 100 μl of WT B38 yeast antibody display library glycerol stock was recovered in 50 ml SD-CAA
390 medium (2% w/v D-glucose, 0.67% w/v yeast nitrogen base with ammonium sulfate, 0.5% w/v
391 casamino acids, 0.54% w/v Na_2HPO_4, 0.86% w/v $NaH_2PO_4 \cdot H_2O$, all dissolved in deionized water)
392 by incubating at 27°C with shaking at 250 rpm until OD_{600} reached between 1.5 and 2.0. At this

bioRxiv preprint doi: https://doi.org/10.1101/2021.01.26.428356; this version posted January 27, 2021. The copyright holder for this preprint (which was not certified by peer review) is the author/funder, who has granted bioRxiv a license to display the preprint in perpetuity. It is made available under aCC-BY 4.0 International license.

393 time, 15 ml of the yeast culture was harvested, and the yeast pellet was obtained via centrifugation
394 at 4,000 × *g* at 4°C for 5 min. The supernatant was discarded, and SGR-CAA (2% w/v galactose,
395 2% w/v raffinose, 0.1% w/v D-glucose, 0.67% w/v yeast nitrogen base with ammonium sulfate,
396 0.5% w/v casamino acids, 0.54% w/v Na_2HPO_4, 0.86% w/v $NaH_2PO_4 \cdot H_2O$, all dissolved in
397 deionized water) was added to make up the volume to 50 ml. The yeast culture was then
398 transferred to a baffled flask and incubated at 18°C with shaking at 250 rpm. Once OD_{600} has
399 reached between 1.3 and 1.6, 1 ml of yeast culture was harvested, and the yeast pellet was
400 obtained via centrifugation at 4,000 × *g* at 4°C for 5 min. The pellet was subsequently washed
401 with 1 ml of 1x PBS twice. After the final wash, cells were resuspended in 1 ml of 1x PBS.
402
403 Then, for expression assay, 1 µg of PE anti-HA.11 (epitope 16B12, BioLegend, Cat. No. 901517)
404 buffer-exchanged into 1x PBS was added to the cells. A negative control was set up with nothing
405 added to the PBS-resuspended cells. Samples were incubated overnight at 4°C with rotation.
406 Then, the yeast pellet was washed twice in 1x PBS and resuspended in FACS tubes containing
407 2 ml 1X PBS. Using a BD FACS Aria II cell sorter (BD Biosciences), PE-positive cells were
408 collected in 1 ml of SD-CAA containing 1x Penicillin/Streptomycin. Cells were then collected via
409 centrifugation at 4,500 rpm at 20°C for 15 min. The supernatant was discarded. Subsequently,
410 the pellet was resuspended in 100 µl of SD-CAA and plated on SD-CAA plates at 37°C. After 40
411 h, colonies were collected in 2 ml of SD-CAA. Frozen stocks were made by reconstituting the
412 pellet in 15% v/v glycerol (in SD-CAA medium) and then stored at -80°C.
413
414 For binding assay, 20 µg of SARS-CoV-2 S RBD-Fc was added to washed cells. A negative
415 control was set up with nothing added to the PBS-resuspended cells. Samples were incubated
416 overnight at 4°C with rotation. The yeast pellet was then washed twice in 1x PBS. After the last
417 wash, cells were resuspended in 1 ml of 1x PBS. Subsequently, 1 µg of PE anti-human IgG Fc

bioRxiv preprint doi: https://doi.org/10.1101/2021.01.26.428356; this version posted January 27, 2021. The copyright holder for this preprint (which was not certified by peer review) is the author/funder, who has granted bioRxiv a license to display the preprint in perpetuity. It is made available under aCC-BY 4.0 International license.

418 antibody (clone HP6017, BioLegend, Cat. No. 409304) buffer-exchanged into 1x PBS was added
419 to yeast. Cells were incubated at 4°C for 1 h with rotation. The yeast pellet was then washed twice
420 in 1x PBS and resuspended in FACS tubes containing 2 ml 1x PBS. Using a BD FACS Aria II cell
421 sorter (BD Biosciences), PE-positive cells were collected in 1 ml of SD-CAA containing 1x
422 Penicillin/Streptomycin. Cells were then collected via centrifugation at 4,500 rpm at 20°C for 15
423 min. The supernatant was then discarded. Subsequently, the pellet was resuspended in 100 µl of
424 SD-CAA and plated on SD-CAA plates at 37°C. After 40 h, colonies were collected in 2 ml of SD-
425 CAA, and subsequently pelleted. Frozen stocks were made by reconstituting yeast pellets with
426 15% v/v glycerol (in SD-CAA medium) and then stored at -80°C.
427

428 **Next-generation sequencing of CDR H3 loops**

429 Plasmids from the unsorted yeast display library (input) as well as two replicates of sorted yeast
430 display library based on RBD-binding and expression were extracted from sorted yeast cells using
431 a Zymoprep Yeast Plasmid Miniprep II Kit (Zymo Research) following the manufacturer's protocol.
432 The CDR H3 region was subsequently amplified via PCR using 5´- ACC TAC AGA TGA ATT CTC
433 TTA GG-3´ and 5´- GGG CCT TTT GTA GAA GCT GAA CT-3´ as forward and reverse primers,
434 respectively. Subsequently, adapters containing sequencing barcodes were appended to the
435 genes encoding the CDR H3 region via PCR. 100 ng of each sample was used for paired-end
436 sequencing using Illumina MiSeq PE150 (Illumina). PEAR was used for merging the forward and
437 reverse reads[82]. Regions corresponding to the CDR H3 were extracted from each paired read.
438 The number of reads corresponding to each CDR H3 variant in each sample is counted. A
439 pseudocount of 1 was added to the final count to avoid division by zero in enrichment calculation.
440 The enrichment for variant *i* was computed as follows:

441
$$\text{Enrichment} = \frac{(\text{read count of variant i in sorted sample})/(\text{total read count in sorted sample})}{(\text{read count of variant i in input})/(\text{total read count in input})}$$

442

bioRxiv preprint doi: https://doi.org/10.1101/2021.01.26.428356; this version posted January 27, 2021. The copyright holder for this preprint (which was not certified by peer review) is the author/funder, who has granted bioRxiv a license to display the preprint in perpetuity. It is made available under aCC-BY 4.0 International license.

443 **Code availability**

444 Custom python scripts for analyzing the deep mutational scanning data have been deposited to
445 https://github.com/wchnicholas/IGHV3-53_sequence_features. Files for Rosetta modeling are
446 available at https://github.com/timothyjtan/ighv3-53_3-66_antibody_sequence_features.
447

448 **Data availability**

449 Raw sequencing data have been submitted to the NIH Short Read Archive under accession
450 number: BioProject PRJNA691562. The X-ray coordinates and structure factors will be deposited
451 to the RCSB Protein Data Bank prior to publication.
452

453 **Acknowledgements**

454 We thank the Roy J. Carver Biotechnology Center at the University of Illinois at Urbana-
455 Champaign for assistance with fluorescence-activated cell sorting and next-generation
456 sequencing. This work was supported by NIH R00 AI139445 (N.C.W.), and Bill and Melinda Gates
457 Foundation INV-004923 (I.A.W.).
458

459 **Competing interests**

460 The authors declare no competing interests.
461

462 **Author Contributions**

463 T.J.C.T., G.C.P. and N.C.W. conceived and designed the study. J.R.B., M.Y. and B.M.S.
464 expressed and purified the proteins. T.J.C.T., K.K., X.C., J.R.C. and C.B.B. performed the yeast
465 display experiments. T.J.C.T., Y.W. and N.C.W. processed the next-generation sequencing data.
466 M.Y. and X.Z. performed the crystallization, X-ray data collection, determined and refined the X-
467 ray structures. T.J.C.T., M.Y., G.C.P., I.A.W. and N.C.W. analyzed the data. T.J.C.T., M.Y., I.A.W.
468 and N.C.W. wrote the paper and all authors reviewed and/or edited the paper.

bioRxiv preprint doi: https://doi.org/10.1101/2021.01.26.428356; this version posted January 27, 2021. The copyright holder for this preprint (which was not certified by peer review) is the author/funder, who has granted bioRxiv a license to display the preprint in perpetuity. It is made available under aCC-BY 4.0 International license.

469 **References**

470 1 Zhou, P. *et al.* A pneumonia outbreak associated with a new coronavirus of probable bat
471 origin. *Nature* **579**, 270-273 (2020).

472 2 Zhu, N. *et al.* A novel coronavirus from patients with pneumonia in China, 2019. *N. Engl.*
473 *J. Med.* **382**, 727-733 (2020).

474 3 Guan, W.-j. *et al.* Clinical characteristics of coronavirus disease 2019 in China. *N. Engl.*
475 *J. Med.* **382**, 1708-1720 (2020).

476 4 Nadim, M. K. *et al.* COVID-19-associated acute kidney injury: consensus report of the
477 25th Acute Disease Quality Initiative (ADQI) Workgroup. *Nat. Rev. Nephrol.* **16**, 1-18
478 (2020).

479 5 Letko, M., Marzi, A. & Munster, V. Functional assessment of cell entry and receptor
480 usage for SARS-CoV-2 and other lineage B betacoronaviruses. *Nat. Microbiol.* **5**, 562-
481 569 (2020).

482 6 Wan, Y., Shang, J., Graham, R., Baric, R. S. & Li, F. Receptor recognition by the novel
483 coronavirus from Wuhan: an analysis based on decade-long structural studies of SARS
484 coronavirus. *J. Virol.* **94**, e00127-00120 (2020).

485 7 Benton, D. J. *et al.* Receptor binding and priming of the spike protein of SARS-CoV-2 for
486 membrane fusion. *Nature* **588**, 327-330 (2020).

487 8 Krammer, F. SARS-CoV-2 vaccines in development. *Nature* **586**, 516-527 (2020).

488 9 Amanat, F. & Krammer, F. SARS-CoV-2 Vaccines: Status Report. *Immunity* **52**, 583-589
489 (2020).

490 10 Polack, F. P. *et al.* Safety and efficacy of the BNT162b2 mRNA Covid-19 vaccine. *N.*
491 *Engl. J. Med.* **383**, 2603-2615 (2020).

492 11 Mahase, E. Covid-19: Moderna vaccine is nearly 95% effective, trial involving high risk
493 and elderly people shows. *BMJ: British Medical Journal (Online)* **371**,
494 doi:https://doi.org/10.1136/bmj.m4471 (2020).

495 12 Mahase, E. Covid-19: Moderna applies for US and EU approval as vaccine trial reports
496 94.1% efficacy. *BMJ: British Medical Journal (Online)* **371**,
497 doi:https://doi.org/10.1136/bmj.m4709 (2020).

498 13 Folegatti, P. M. *et al.* Safety and immunogenicity of the ChAdOx1 nCoV-19 vaccine
499 against SARS-CoV-2: a preliminary report of a phase 1/2, single-blind, randomised
500 controlled trial. *Lancet* **396**, 467-478 (2020).

501 14 Ramasamy, M. N. *et al.* Safety and immunogenicity of ChAdOx1 nCoV-19 vaccine
502 administered in a prime-boost regimen in young and old adults (COV002): a single-blind,
503 randomised, controlled, phase 2/3 trial. *Lancet* **396**, 1979-1993 (2020).

bioRxiv preprint doi: https://doi.org/10.1101/2021.01.26.428356; this version posted January 27, 2021. The copyright holder for this preprint (which was not certified by peer review) is the author/funder, who has granted bioRxiv a license to display the preprint in perpetuity. It is made available under aCC-BY 4.0 International license.

504 505 506 15 Voysey, M. *et al.* Safety and efficacy of the ChAdOx1 nCoV-19 vaccine (AZD1222) against SARS-CoV-2: an interim analysis of four randomised controlled trials in Brazil, South Africa, and the UK. *Lancet* **397**, 99-111 (2021).

507 508 509 16 Premkumar, L. *et al.* The receptor binding domain of the viral spike protein is an immunodominant and highly specific target of antibodies in SARS-CoV-2 patients. *Sci. Immunol.* **5**, doi:https://doi.org/10.1126/sciimmunol.abc8413 (2020).

510 511 512 17 Yuan, M., Liu, H., Wu, N. C. & Wilson, I. A. Recognition of the SARS-CoV-2 receptor binding domain by neutralizing antibodies. *Biochem. Biophys. Res. Commun.*, doi:https://doi.org/10.1016/j.bbrc.2020.10.012 (2020).

513 514 18 Jiang, S., Hillyer, C. & Du, L. Neutralizing antibodies against SARS-CoV-2 and other human coronaviruses. *Trends Immunol.* **41**, 355-359 (2020).

515 516 19 Wajnberg, A. *et al.* Robust neutralizing antibodies to SARS-CoV-2 infection persist for months. *Science* **370**, 1227-1230 (2020).

517 518 20 Yuan, M. *et al.* A highly conserved cryptic epitope in the receptor binding domains of SARS-CoV-2 and SARS-CoV. *Science* **368**, 630-633 (2020).

519 520 21 Pinto, D. *et al.* Cross-neutralization of SARS-CoV-2 by a human monoclonal SARS-CoV antibody. *Nature* **583**, 290-295 (2020).

521 522 22 Ju, B. *et al.* Human neutralizing antibodies elicited by SARS-CoV-2 infection. *Nature* **584**, 115-119 (2020).

523 524 525 23 Cao, Y. *et al.* Potent neutralizing antibodies against SARS-CoV-2 identified by high-throughput single-cell sequencing of convalescent patients' B cells. *Cell* **182**, 73-84 (2020).

526 527 24 Rogers, T. F. *et al.* Isolation of potent SARS-CoV-2 neutralizing antibodies and protection from disease in a small animal model. *Science* **369**, 956-963 (2020).

528 529 25 Brouwer, P. J. M. *et al.* Potent neutralizing antibodies from COVID-19 patients define multiple targets of vulnerability. *Science* **369**, 643-650 (2020).

530 531 26 Wu, Y. *et al.* A noncompeting pair of human neutralizing antibodies block COVID-19 virus binding to its receptor ACE2. *Science* **368**, 1274-1278 (2020).

532 533 27 Chi, X. *et al.* A neutralizing human antibody binds to the N-terminal domain of the Spike protein of SARS-CoV-2. *Science* **369**, 650-655 (2020).

534 535 28 Seydoux, E. *et al.* Characterization of neutralizing antibodies from a SARS-CoV-2 infected individual. *bioRxiv*, doi:https://doi.org/10.1101/2020.05.12.091298 (2020).

536 537 29 Shi, R. *et al.* A human neutralizing antibody targets the receptor-binding site of SARS-CoV-2. *Nature* **584**, 120-124 (2020).

538 539 30 Wan, J. *et al.* Human-IgG-neutralizing monoclonal antibodies block the SARS-CoV-2 infection. *Cell Rep.* **32**, 107918 (2020).

bioRxiv preprint doi: https://doi.org/10.1101/2021.01.26.428356; this version posted January 27, 2021. The copyright holder for this preprint (which was not certified by peer review) is the author/funder, who has granted bioRxiv a license to display the preprint in perpetuity. It is made available under aCC-BY 4.0 International license.

540 31 Barnes, C. O. *et al.* Structures of human antibodies bound to SARS-CoV-2 spike reveal
541 common epitopes and recurrent features of antibodies. *Cell* **182**, 828-842 (2020).

542 32 Robbiani, D. F. *et al.* Convergent antibody responses to SARS-CoV-2 in convalescent
543 individuals. *Nature* **584**, 437-442 (2020).

544 33 Han, X. *et al.* A rapid and efficient screening system for neutralizing antibodies and its
545 application for the discovery of potent neutralizing antibodies to SARS-CoV-2 S-RBD.
546 *bioRxiv*, doi:https://doi.org/10.1101/2020.08.19.253369 (2020).

547 34 Kreye, J. *et al.* A therapeutic non-self-reactive SARS-CoV-2 antibody protects from lung
548 pathology in a COVID-19 hamster model. *Cell* **183**, 1058-1069 (2020).

549 35 Zost, S. J. *et al.* Rapid isolation and profiling of a diverse panel of human monoclonal
550 antibodies targeting the SARS-CoV-2 spike protein. *Nat. Med.* **26**, 1422-1427 (2020).

551 36 Liu, L. *et al.* Potent neutralizing antibodies against multiple epitopes on SARS-CoV-2
552 spike. *Nature* **584**, 450-456 (2020).

553 37 Kreer, C. *et al.* Longitudinal isolation of potent near-germline SARS-CoV-2-neutralizing
554 antibodies from COVID-19 patients. *Cell* **182**, 843-854 (2020).

555 38 Hurlburt, N. K. *et al.* Structural basis for potent neutralization of SARS-CoV-2 and role of
556 antibody affinity maturation. *Nat. Commun.* **11**, 5413 (2020).

557 39 Noy-Porat, T. *et al.* A panel of human neutralizing mAbs targeting SARS-CoV-2 spike at
558 multiple epitopes. *Nat. Commun.* **11**, 4303 (2020).

559 40 Du, S. *et al.* Structurally resolved SARS-CoV-2 antibody shows high efficacy in severely
560 infected hamsters and provides a potent cocktail pairing strategy. *Cell* **183**, 1013-1023
561 (2020).

562 41 Hozumi, N. & Tonegawa, S. Evidence for somatic rearrangement of immunoglobulin
563 genes coding for variable and constant regions. *Proc. Natl. Acad. Sci. U. S. A.* **73**, 3628-
564 3632 (1976).

565 42 Brack, C., Hirama, M., Lenhard-Schuller, R. & Tonegawa, S. A complete immunoglobulin
566 gene is created by somatic recombination. *Cell* **15**, 1-14 (1978).

567 43 Seidman, J. *et al.* Multiple related immunoglobulin variable-region genes identified by
568 cloning and sequence analysis. *Proc. Natl. Acad. Sci. U. S. A.* **75**, 3881-3885 (1978).

569 44 Bernard, O., Hozumi, N. & Tonegawa, S. Sequences of mouse immunoglobulin light
570 chain genes before and after somatic changes. *Cell* **15**, 1133-1144 (1978).

571 45 O'Brien, R., Brinster, R. & Storb, U. Somatic hypermutation of an immunoglobulin
572 transgene in K transgenic mice. *Nature* **326**, 405-409 (1987).

573 46 Nielsen, S. C. A. *et al.* Human B cell clonal expansion and convergent antibody
574 responses to SARS-CoV-2. *Cell Host Microbe* **28**, 516-525 (2020).

bioRxiv preprint doi: https://doi.org/10.1101/2021.01.26.428356; this version posted January 27, 2021. The copyright holder for this preprint (which was not certified by peer review) is the author/funder, who has granted bioRxiv a license to display the preprint in perpetuity. It is made available under aCC-BY 4.0 International license.

575 47 Yuan, M. *et al.* Structural basis of a shared antibody response to SARS-CoV-2. *Science*
576 **369**, 1119-1123 (2020).

577 48 Setliff, I. *et al.* Multi-donor longitudinal antibody repertoire sequencing reveals the
578 existence of public antibody clonotypes in HIV-1 infection. *Cell Host Microbe* **23**, 845-
579 854 (2018).

580 49 Jackson, K. J. *et al.* Human responses to influenza vaccination show seroconversion
581 signatures and convergent antibody rearrangements. *Cell Host Microbe* **16**, 105-114
582 (2014).

583 50 Trück, J. *et al.* Identification of antigen-specific B cell receptor sequences using public
584 repertoire analysis. *J. Immunol.* **194**, 252-261 (2015).

585 51 Dunand, C. J. H. & Wilson, P. C. Restricted, canonical, stereotyped and convergent
586 immunoglobulin responses. *Philos. Trans. R. Soc. Lond., Ser. B: Biol. Sci.* **370**,
587 20140238 (2015).

588 52 Pieper, K. *et al.* Public antibodies to malaria antigens generated by two LAIR1 insertion
589 modalities. *Nature* **548**, 597-601 (2017).

590 53 Parameswaran, P. *et al.* Convergent antibody signatures in human dengue. *Cell Host*
591 *Microbe* **13**, 691-700 (2013).

592 54 Wu, N. C. *et al.* An alternative binding mode of IGHV3-53 antibodies to the SARS-CoV-2
593 receptor binding domain. *Cell Rep.* **33**, 108274 (2020).

594 55 Barnes, C. O. *et al.* SARS-CoV-2 neutralizing antibody structures inform therapeutic
595 strategies. *Nature* **588**, 682-687 (2020).

596 56 Bertoglio, F. *et al.* A SARS-CoV-2 neutralizing antibody selected from COVID-19
597 patients by phage display is binding to the ACE2-RBD interface and is tolerant to known
598 RBD mutations. *bioRxiv*, doi:https://doi.org/10.1101/2020.12.03.409318 (2020).

599 57 Clark, S. A. *et al.* Molecular basis for a germline-biased neutralizing antibody response
600 to SARS-CoV-2. *bioRxiv*, doi:https://doi.org/10.1101/2020.11.13.381533 (2020).

601 58 Sinnokrot, M. O., Valeev, E. F. & Sherrill, C. D. Estimates of the ab initio limit for π−π
602 interactions: The benzene dimer. *J. Am. Chem. Soc.* **124**, 10887-10893 (2002).

603 59 Chelli, R., Gervasio, F. L., Procacci, P. & Schettino, V. Stacking and T-shape
604 competition in aromatic−aromatic amino acid interactions. *J. Am. Chem. Soc.* **124**, 6133-
605 6143 (2002).

606 60 Kim, S. I. *et al.* Stereotypic neutralizing VH antibodies against SARS-CoV-2 spike
607 protein receptor binding domain in COVID-19 patients and healthy individuals. *Sci.*
608 *Transl. Med.*, doi:https://doi.org/10.1126/scitranslmed.abd6990 (2021).

609 61 Banach, B. B. *et al.* Paired heavy and light chain signatures contribute to potent SARS-
610 CoV-2 neutralization in public antibody responses. *bioRxiv*,
611 doi:https://doi.org/10.1101/2020.12.31.424987 (2021).

bioRxiv preprint doi: https://doi.org/10.1101/2021.01.26.428356; this version posted January 27, 2021. The copyright holder for this preprint (which was not certified by peer review) is the author/funder, who has granted bioRxiv a license to display the preprint in perpetuity. It is made available under aCC-BY 4.0 International license.

612 62 Gaebler, C. *et al.* Evolution of antibody immunity to SARS-CoV-2. *Nature*,
613 doi:https://doi.org/10.1038/s41586-021-03207-w (2021).

614 63 Tegally, H. *et al.* Emergence and rapid spread of a new severe acute respiratory
615 syndrome-related coronavirus 2 (SARS-CoV-2) lineage with multiple spike mutations in
616 South Africa. *medRxiv*, doi:https://doi.org/10.1101/2020.12.21.20248640 (2020).

617 64 Voloch, C. M. *et al.* Genomic characterization of a novel SARS-CoV-2 lineage from Rio
618 de Janeiro, Brazil. *medRxiv*, doi:https://doi.org/10.1101/2020.12.23.20248598 (2020).

619 65 Weisblum, Y. *et al.* Escape from neutralizing antibodies by SARS-CoV-2 spike protein
620 variants. *eLife* **9**, e61312 (2020).

621 66 Greaney, A. J. *et al.* Complete mapping of mutations to the SARS-CoV-2 spike receptor-
622 binding domain that escape antibody recognition. *Cell Host Microbe* **29**, 44-57 (2021).

623 67 Andreano, E. *et al.* SARS-CoV-2 escape in vitro from a highly neutralizing COVID-19
624 convalescent plasma. *bioRxiv*, doi:https://doi.org/10.1101/2020.12.28.424451 (2020).

625 68 Buss, L. F. *et al.* Three-quarters attack rate of SARS-CoV-2 in the Brazilian Amazon
626 during a largely unmitigated epidemic. *Science* **371**, 288-292 (2021).

627 69 Greaney, A. J. *et al.* Comprehensive mapping of mutations to the SARS-CoV-2 receptor-
628 binding domain that affect recognition by polyclonal human serum antibodies. *bioRxiv*,
629 doi:https://doi.org/10.1101/2020.12.31.425021 (2021).

630 70 Wang, Z. *et al.* mRNA vaccine-elicited antibodies to SARS-CoV-2 and circulating
631 variants. *bioRxiv*, 2021.2001.2015.426911, doi:10.1101/2021.01.15.426911 (2021).

632 71 Wibmer, C. K. *et al.* SARS-CoV-2 501Y.V2 escapes neutralization by South African
633 COVID-19 donor plasma. *bioRxiv*, 2021.2001.2018.427166,
634 doi:10.1101/2021.01.18.427166 (2021).

635 72 Ye, J., Ma, N., Madden, T. L. & Ostell, J. M. IgBLAST: an immunoglobulin variable
636 domain sequence analysis tool. *Nucleic Acids Res.* **41**, W34-W40 (2013).

637 73 Crooks, G. E., Hon, G., Chandonia, J.-M. & Brenner, S. E. WebLogo: a sequence logo
638 generator. *Genome Res.* **14**, 1188-1190 (2004).

639 74 Wu, N. C. *et al.* In vitro evolution of an influenza broadly neutralizing antibody is
640 modulated by hemagglutinin receptor specificity. *Nat. Commun.* **8**, 15371 (2017).

641 75 Otwinowski, Z. & Minor, W. Processing of X-ray diffraction data collected in oscillation
642 mode. *Methods Enzymol.* **276**, 307-326 (1997).

643 76 McCoy, A. J. *et al.* Phaser crystallographic software. *J. Appl. Crystallogr.* **40**, 658-674
644 (2007).

645 77 Schritt, D. *et al.* Repertoire Builder: high-throughput structural modeling of B and T cell
646 receptors. *Mol. Syst. Des. Eng.* **4**, 761-768, doi:10.1039/C9ME00020H (2019).

bioRxiv preprint doi: https://doi.org/10.1101/2021.01.26.428356; this version posted January 27, 2021. The copyright holder for this preprint (which was not certified by peer review) is the author/funder, who has granted bioRxiv a license to display the preprint in perpetuity. It is made available under aCC-BY 4.0 International license.

647 78 Emsley, P., Lohkamp, B., Scott, W. G. & Cowtan, K. Features and development of Coot.
648 *Acta Crystallogr. D Biol. Crystallogr.* **66**, 486-501 (2010).

649 79 Adams, P. D. *et al.* PHENIX: a comprehensive Python-based system for macromolecular
650 structure solution. *Acta Crystallogr. D Biol. Crystallogr.* **66**, 213-221 (2010).

651 80 Chao, G. *et al.* Isolating and engineering human antibodies using yeast surface display.
652 *Nat. Protoc.* **1**, 755 (2006).

653 81 Benatuil, L., Perez, J. M., Belk, J. & Hsieh, C.-M. An improved yeast transformation
654 method for the generation of very large human antibody libraries. *Protein Eng. Des. Sel.*
655 **23**, 155-159 (2010).

656 82 Zhang, J., Kobert, K., Flouri, T. & Stamatakis, A. PEAR: a fast and accurate Illumina
657 Paired-End reAd mergeR. *Bioinformatics* **30**, 614-620 (2014).

658 83 Kovaltsuk, A. *et al.* Observed antibody space: A resource for data mining next-
659 generation sequencing of antibody repertoires. *J. Immunol.* **201**, 2502-2509 (2018).
660

bioRxiv preprint doi: https://doi.org/10.1101/2021.01.26.428356; this version posted January 27, 2021. The copyright holder for this preprint (which was not certified by peer review) is the author/funder, who has granted bioRxiv a license to display the preprint in perpetuity. It is made available under aCC-BY 4.0 International license.

661 **Figures**

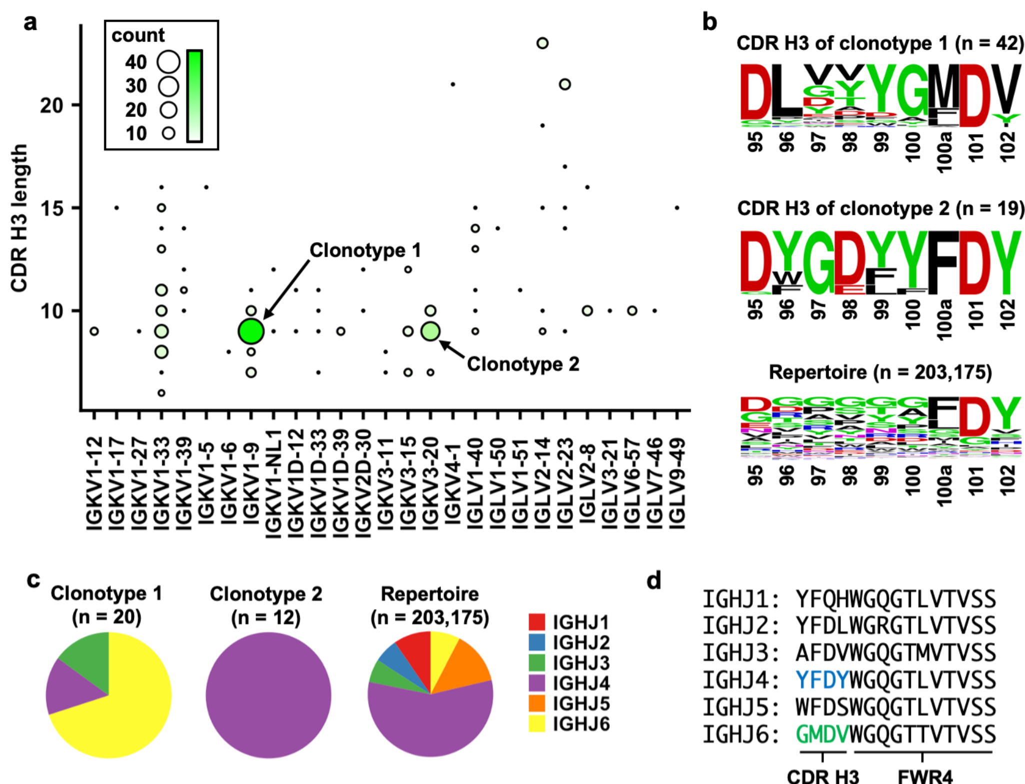

662

663 **Figure 1. Two major clonotypes of IGHV3-53/3-66 antibodies to SARS-CoV-2 RBD. (a)** The
664 number of IGHV3-53/3-66 RBD antibodies that use the same light chain with the same CDR H3
665 are tabulated. The two most common combinations are IGKV1-9 pairing with 9 aa CDR H3 and
666 IGKV3-20 pairing with 9 aa CDR H3, denoted as clonotype 1 and clonotype 2, respectively. **(b)**
667 Sequence logos for the CDR H3 regions of IGHV3-53/66 antibodies that pair with IGKV1-9 or
668 IGKV3-20. A sequence logo for the CDR H3 regions of 203,175 IGHV3-53/3-66 antibodies from
669 Observed Antibody Space database[83] that have a CDR H3 length of 9 aa is shown for reference
670 (repertoire). The position of each residue is labeled on the x-axis based on Kabat numbering. **(c)**
671 IGHJ gene usage for clonotypes 1 and 2 as well as 203,175 IGHV3-53/3-66 antibodies from
672 Observed Antibody Space database that have a CDR H3 length of 9 aa (repertoire) are shown
673 as pie charts. For antibodies in clonotypes 1 and 2, only those with nucleotide sequence
674 information available were analyzed. **(d)** Amino acid sequences for different IGHJs are shown.

bioRxiv preprint doi: https://doi.org/10.1101/2021.01.26.428356; this version posted January 27, 2021. The copyright holder for this preprint (which was not certified by peer review) is the author/funder, who has granted bioRxiv a license to display the preprint in perpetuity. It is made available under aCC-BY 4.0 International license.

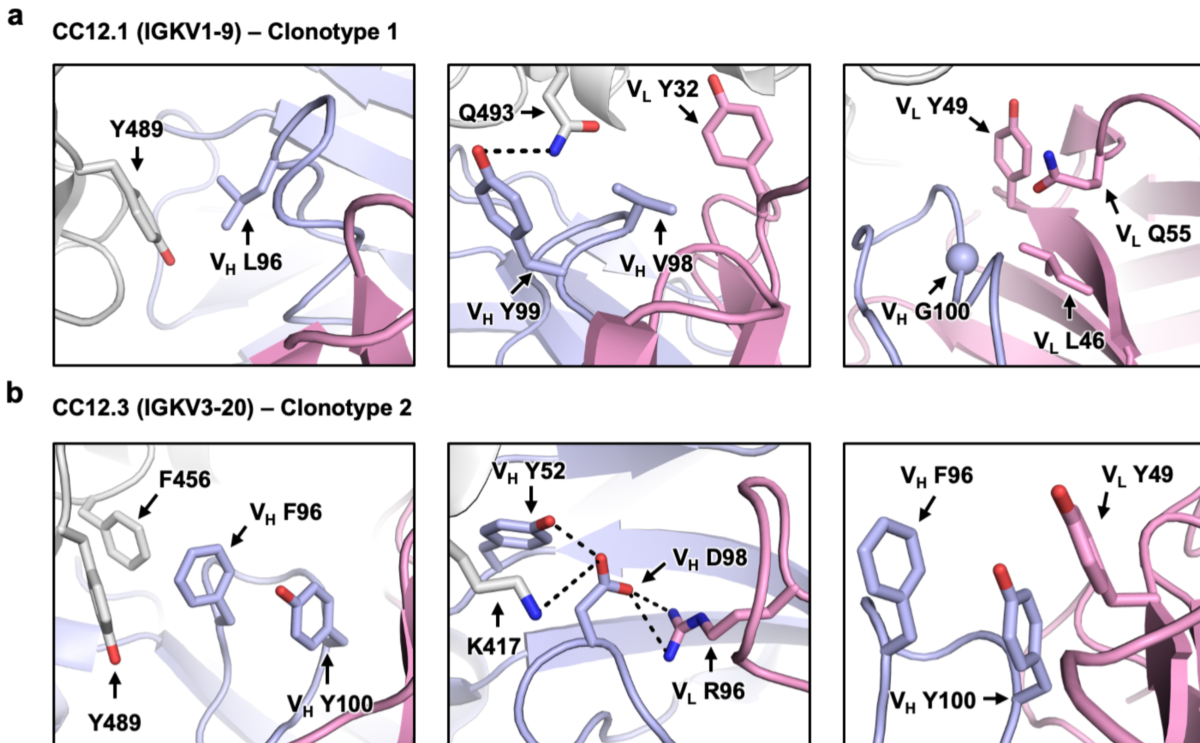

675

676 **Figure 2. Structural analysis of sequence signatures in CDR H3 of clonotypes 1 and 2. (a)**
677 Interaction of L96, V98 and G100 (Kabat numbering) in CDR H3 of CC12.1 (PDB 6XC2) with the
678 IGKV1-9 light chain of the antibody, and SARS-CoV-2 RBD. **(b)** Interaction of F96, D98 and Y100
679 (Kabat numbering) in CDR H3 of CC12.3 (PDB 6XC4) with the IGKV3-20 light chain of the
680 antibody, and SARS-CoV-2 RBD. Gray: RBD; Light blue: heavy chain; Pink: light chain.

bioRxiv preprint doi: https://doi.org/10.1101/2021.01.26.428356; this version posted January 27, 2021. The copyright holder for this preprint (which was not certified by peer review) is the author/funder, who has granted bioRxiv a license to display the preprint in perpetuity. It is made available under aCC-BY 4.0 International license.

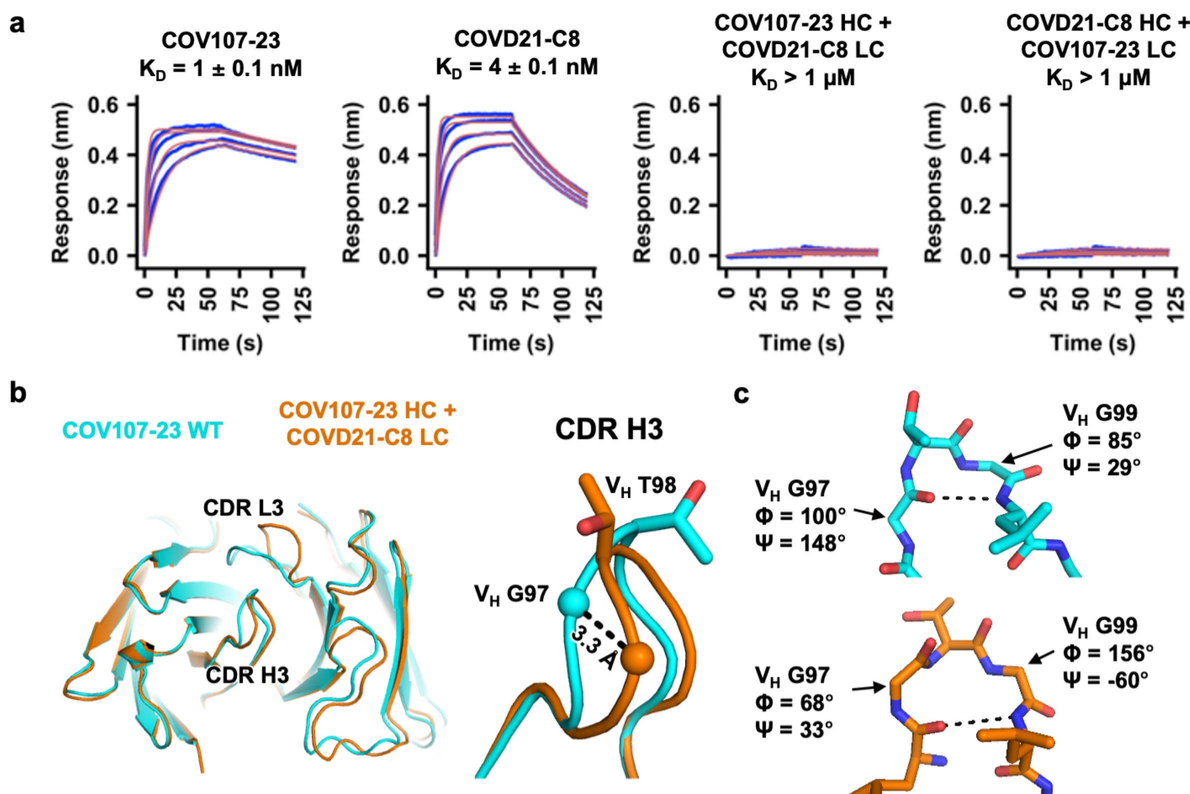

681

682 **Figure 3. Specific pairing of CDR H3 and light chain is critical for IGHV3-53/3-66 antibody**
683 **binding to SARS-CoV-2 RBD. (a)** Binding of different Fabs to SARS-CoV-2 RBD was measured
684 by biolayer interferometry with RBD loaded onto the biosensor and Fab in solution. Y-axis
685 represents the response. Dissociation constant (K_D) for each Fab was obtained using a 1:1
686 binding model, which is represented by the red curves. **(b)** Fab crystal structures of wild-type (WT)
687 COV107-23 and COV107-23 heavy chain pairing with COVD21-C8 light chain are compared. Left
688 panel: structural alignment using residues 1-90 of the heavy chain. Right panel: Zoom-in view for
689 the CDR H3. **(c)** Conformations at the tips of the CDR H3s in WT COV107-23 and COV107-23
690 heavy chain pairing with COVD21-C8 light chain are shown. A β-turn is observed in the CDR H3
691 of WT COV107-23, with V_H G97 and V_H G99 at i and i+2 positions, respectively.

bioRxiv preprint doi: https://doi.org/10.1101/2021.01.26.428356; this version posted January 27, 2021. The copyright holder for this preprint (which was not certified by peer review) is the author/funder, who has granted bioRxiv a license to display the preprint in perpetuity. It is made available under aCC-BY 4.0 International license.

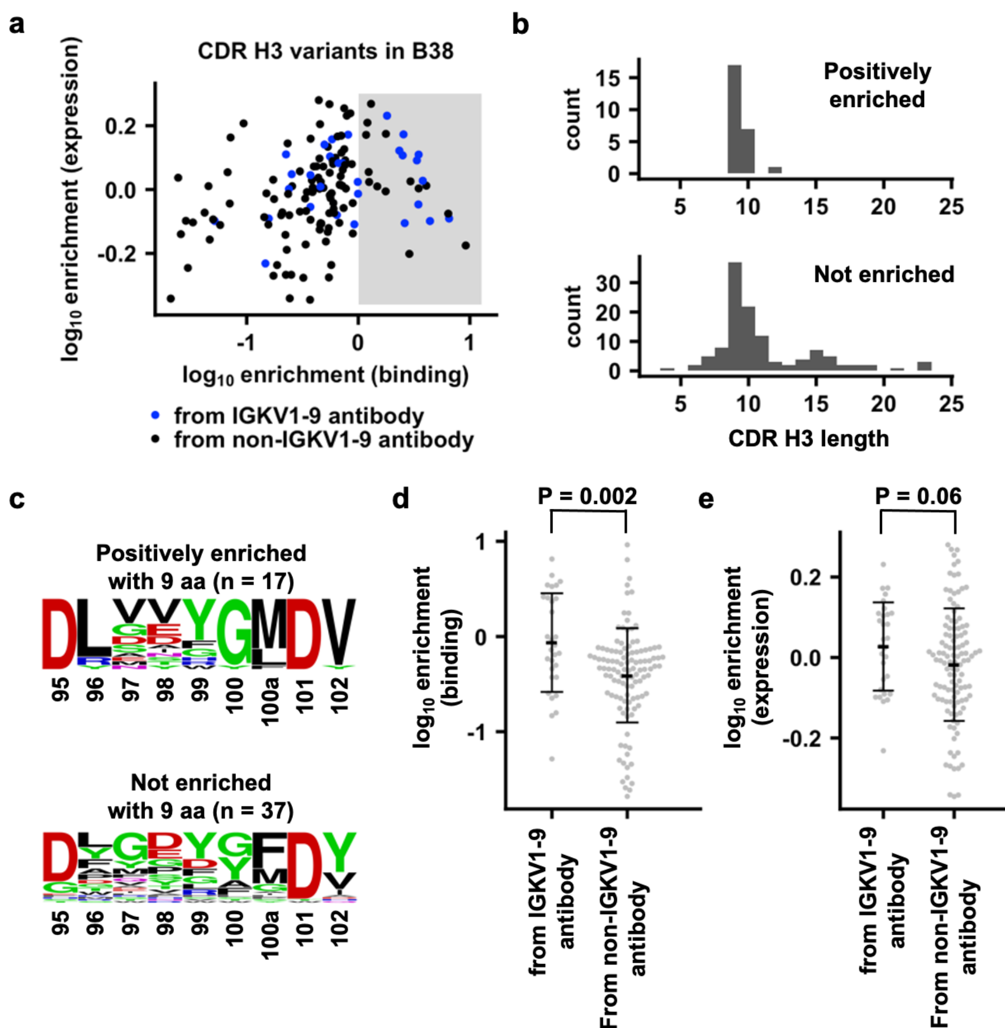

692

693 **Figure 4. Binding and expression profiling of 143 CDR H3 variants in B38 antibody. (a)** For
694 each of the 143 CDR H3 variants, the enrichment in occurrence frequencies after FACS
695 selections for binding to RBD and expression level are shown. Blue: CDR H3 variants that are
696 derived from IGHV3-53/3-66 RBD antibodies that use IGKV1-9. Black: CDR H3 variants that are
697 derived from IGHV3-53/3-66 RBD antibodies that do not use IGKV1-9. Shaded area indicates
698 $\log_{10}$ enrichment in binding > 0. **(b)** The amino-acid length distribution of CDR H3 variants that
699 are positively enriched in binding ($\log_{10}$ enrichment in binding > 0) or not ($\log_{10}$ enrichment in
700 binding ≤ 0) is shown. **(c)** Sequence logos are shown for CDR H3 variants with 9 aa (Kabat
701 numbering) that are positively enriched or not enriched. **(d)** Comparison of $\log_{10}$ enrichment in

bioRxiv preprint doi: https://doi.org/10.1101/2021.01.26.428356; this version posted January 27, 2021. The copyright holder for this preprint (which was not certified by peer review) is the author/funder, who has granted bioRxiv a license to display the preprint in perpetuity. It is made available under aCC-BY 4.0 International license.

702 binding for CDR H3 variants from IGHV3-53/3-66 RBD antibodies that use IGKV1-9 and those
703 that do not use IGKV1-9. **(e)** Comparison of $\log_{10}$ enrichment in expression for CDR H3 variants
704 from IGHV3-53/3-66 RBD antibodies that use IGKV1-9 and those that do not use IGKV1-9. **(d-e)**
705 Student's t-test was used to compute the p-value.

bioRxiv preprint doi: https://doi.org/10.1101/2021.01.26.428356; this version posted January 27, 2021. The copyright holder for this preprint (which was not certified by peer review) is the author/funder, who has granted bioRxiv a license to display the preprint in perpetuity. It is made available under aCC-BY 4.0 International license.

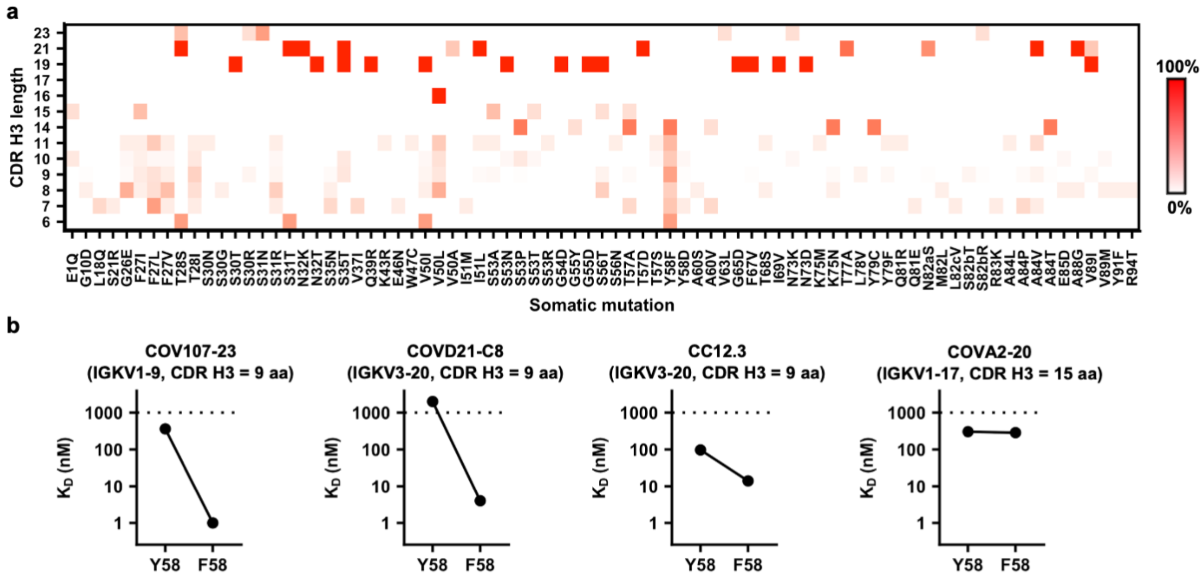

706

707 **Figure 5. Y58F is a signature somatic hypermutation in IGHV3-53/3-66 RBD antibodies with**
708 **a short CDR H3. (a)** IGHV3-53/3-66 RBD antibodies are categorized based on their CDR H3
709 length (Kabat numbering). Occurrence frequencies of individual somatic hypermutations in
710 different categories were quantified and shown as a heatmap. **(b)** Both Y58 and F58 variants
711 were constructed for four IGHV3-53 antibodies. Binding affinity (K_D) of each of these antibodies
712 as Fab format to SARS-CoV-2 RBD was measured by biolayer interferometry with RBD loaded
713 on the biosensor and Fab in solution. Y-axis represents the response. Dissociation constants (K_D)
714 for the Fabs were obtained using a 1:1 binding model. Of note, the WTs of COV107-23, COVD21-
715 C8, and CC12.3 contain F58, whereas the WT of COVA2-20 contains Y58.